Research Article

First PET Imaging Studies With ^{63}Zn-Zinc Citrate in Healthy Human Participants and Patients With Alzheimer Disease

Timothy R. DeGrado, PhD[1], Bradley J. Kemp, PhD[1], Mukesh K. Pandey, PhD[1], Huailei Jiang, PhD[1], Tina M. Gunderson, MS[2], Logan R. Linscheid, CNMT[1], Allison R. Woodwick, CNMT[1], Daniel M. McConnell, CNMT[1], Joel G. Fletcher, MD[1], Geoffrey B. Johnson, MD, PhD[1], Ronald C. Petersen, MD, PhD[3], David S. Knopman, MD[3], and Val J. Lowe, MD[1]

Abstract

Abnormalities in zinc homeostasis are indicated in many human diseases, including Alzheimer disease (AD). ^{63}Zn-zinc citrate was developed as a positron emission tomography (PET) imaging probe of zinc transport and used in a first-in-human study in 6 healthy elderly individuals and 6 patients with clinically confirmed AD. Dynamic PET imaging of the brain was performed for 30 minutes following intravenous administration of ^{63}Zn-zinc citrate ($\sim$330 MBq). Subsequently, body PET images were acquired. Urine and venous blood were analyzed to give information on urinary excretion and pharmacokinetics. Regional cerebral ^{63}Zn clearances were compared with ^{11}C-Pittsburgh Compound B (^{11}C-PiB) and ^{18}F-fluorodeoxyglucose (^{18}F-FDG) imaging data. ^{63}Zn-zinc citrate was well tolerated in human participants with no adverse events monitored. Tissues of highest uptake were liver, pancreas, and kidney, with moderate uptake being seen in intestines, prostate (in males), thyroid, spleen, stomach, pituitary, and salivary glands. Moderate brain uptake was observed, and regional dependencies were observed in ^{63}Zn clearance kinetics in relationship with regions of high amyloid-β plaque burden (^{11}C-PiB) and ^{18}F-FDG hypometabolism. In conclusion, zinc transport was successfully imaged in human participants using the PET probe ^{63}Zn-zinc citrate. Primary sites of uptake in the digestive system accent the role of zinc in gastrointestinal function. Preliminary information on zinc kinetics in patients with AD evidenced regional differences in clearance rates in correspondence with regional amyloid-β pathology, warranting further imaging studies of zinc homeostasis in patients with AD.

Zinc is an essential metal in the body, which is a functional requirement for more than 300 metabolic enzymes and plays fundamental roles in protein structure and protein–protein interactions.[1] The tertiary, quaternary, and quinary structures of proteins depend on zinc and other metal ions, which in turn affect protein aggregation and protein interactions with other proteins, DNA/RNA, and lipids. Zinc deficiency is a nutritional disorder affecting approximately 2 billion people in the developing world,[2] while excess zinc consumption can cause detrimental effects of ataxia, lethargy, and copper deficiency. Abnormalities in zinc homeostasis have been implied in metabolic syndrome, diabetes, and diabetic complications.[3] Zinc homeostasis may play an important role in certain cancer types, including pancreatic cancer,[4] prostate cancer,[5] and breast cancer.[6] Also, zinc is associated with the aggregation of β-amyloid proteins that accumulate in brains of patients with Alzheimer

disease (AD).[7] Metal chelation therapy is under investigation for the treatment of AD, with the intent of altering zinc and copper binding within amyloid-β protein deposits in the brain.[8] A recent study suggests that AD may have 3 distinct subtypes with regard to pathophysiology, with 1 being associated with zinc deficiency.[9]

[1] Department of Radiology, Mayo Clinic, Rochester, MN, USA
[2] Department of Health Sciences Research, Mayo Clinic, Rochester, MN, USA
[3] Department of Neurology, Mayo Clinic, Rochester, MN, USA

Corresponding Author:
Timothy R. DeGrado, Molecular Imaging Research, Mayo Clinic, 200 First Street SW, Rochester, MN 55905, USA.
E-mail: degrado.timothy@mayo.edu

The potential role of positron emission tomography (PET) imaging in assessing metal homeostasis in brains of patients with AD has recently motivated the development of ^{18}F-CABS13 as a zinc ionophore molecule that is able to permeate the blood–brain barrier (BBB) and shows differences in brain uptake in APP/PS1 mice relative to age-matched wild-type mice.[10] Clearly, information on the dynamics of the metal ions themselves in preclinical models of AD and in patients with AD would provide important information that could support (or call into question) the so-called "metals hypothesis" of AD.[11] According to this hypothesis, zinc and copper may play a key role in the formation and stabilization of neurotoxic oligomers of amyloid β-proteins.[11] To address this need, we have recently developed [63]Zn-zinc citrate as a PET probe of zinc transport.[12] The 38.5-minute radioisotopic half-life of [63]Zn allows imaging studies of duration up to 2 to 3 hours to evaluate biodistribution and moderately rapid turnover processes in tissues. Biodistribution of [63]Zn-zinc citrate in mice was found to be predominantly within the gastrointestinal (GI) tract, with low but significant uptake in brain regions.[12]

In the present study, we report data for the first time on [63]Zn-zinc kinetics obtained in human participants. The biodistribution of [63]Zn-zinc in the form of zinc citrate was assessed by PET imaging in healthy elderly individuals and in patients with AD after intravenous administration of radiotracer. Attention was paid to the measurement of cerebral uptake and clearance kinetics in order to evaluate any differences in zinc kinetics in patients with AD relative to healthy individuals. The studies show extensive distribution of [63]Zn-zinc citrate in the liver, pancreas, and GI tract, with certain differences in regional brain kinetics in patients with AD corresponding to the known regional amyloid-β pathology.

Methods

Preparation of [63]Zn-Zinc Citrate

[63]Zn was produced in a low-energy cyclotron (GE PETtrace, GE HealthCare, Waukesha, WI) via the [63]Cu(*p, n*)[63]Zn reaction in an in-house-developed solution target, as previously described.[12] The final product, [63]Zn-zinc citrate was prepared using an isotonic 4% sodium citrate United States Pharmacopeia solution (Fenwal Inc, Lake Zurich, Illinois) and passed standard quality control tests for Current Good Manufacturing Practice for radiopharmaceutical production.[12] Specific activity of [63]Zn in the radiopharmaceutical product was 19.4 ± 14.6 GBq/μmol at the end of synthesis. Iron and copper ions were present at concentrations of 2.7 ± 2.5 mg/L and 0.18 ± 0.16 mg/L, respectively. Injection volumes ranged from 3 to 7 mL.

Human Participants

From April 2014 to September 2014, 6 healthy elderly individuals (2 males and 4 females; age 55-77) and 6 patients with AD (3 males and 3 females; age 63-88) were enrolled into the study. The participant characteristics are shown in Table 1. All patients were participants of an ongoing clinical trial on imaging evaluation of AD within the Mayo Clinic Alzheimer's Research Center and had undergone clinical and

imaging diagnostic (magnetic resonance [MR], ^{11}C-Pittsburgh Compound B [^{11}C-PiB]PET and ^{18}F-fluorodeoxyglucose [^{18}F-FDG]PET) testing within the last 9 months prior to the study. Healthy participants showed no evidence of AD-related abnormalities on ^{11}C-PiB-PET or ^{18}F-FDG-PET scans indicative of AD. All patients with AD met the National Institute of Neurological and Communicative Disorders and Stroke (NINCDS) criteria for probable AD and had a Mini-Mental State Examination score at screening between 10 and 24 inclusive. All participants were given the Short Test of Mental Status (STMS). The mean STMS score for healthy participants and patients with AD was 36.3/38 and 19.0/38, respectively. Patients with AD also had unequivocal evidence of amyloid-β plaque burden on ^{11}C-PiB-PET. All participants were requested to abstain from intake of food, vitamins, and cough medications that contain zinc beginning from 8 PM in the evening prior to the study. Participants were instructed to maintain fasting but drink plenty of water in the morning prior to the study to be well hydrated. [63]Zn-zinc citrate was administered at about 11 AM on the day of the study. The study protocol was approved by the institutional review board of the Mayo Clinic, and all participants provided informed consent.

Imaging Protocol

The imaging protocol is illustrated in Figure 1. After voiding of the bladder, participants were positioned in a GE 690XT PET/computed tomography (CT) scanner (GE HealthCare, Waukesha, WI) in a supine position. Intravenous catheters were placed in both arms for radiotracer injection and blood sampling. Computed tomography scans of the head were initially acquired in the preparation for a dynamic PET data acquisition over the brain for the first 30 minutes following commencement of intravenous administration. [63]Zn-zinc citrate (300-370 MBq) was administered over 1 minute into one of the venous catheters. The frame sequence for the initial dynamic PET acquisition was 15×4, 8×15, 4×30, and 5×300 seconds. Following the dynamic brain scan, the participants were allowed a 15-minute break from the scanner, during which time voided their bladders. Two subsequent head to thigh (trunk) PET/CT scans were acquired at 45 to 70 minutes and 95 to 120 minutes postinjection (PI) with 15 to 20 minutes of break in between. The last PET/CT scan was completed at ∼2 hours PI. Venous blood samples (3-4 mL) were collected in heparinized tubes and placed on ice, beginning at 5 minutes PI and continuing over the imaging period. Urine was collected after each PET scan and measured for urine volume and [63]Zn concentration as measured in a calibrated γ counter.

Measurements in Venous Blood and Urine Samples

Ice-chilled blood samples were centrifuged at 3000*g* for 5 minutes to obtain plasma. [63]Zn concentrations in whole blood and plasma were measured using a calibrated γ counter. [63]Zn excretion in urine was calculated from the product of urine volume and [63]Zn concentration.

Table 1. Participant Characteristics, Clinical Parameters, and Cognitive Test Results.

Participant	Sex (F/M)	Age, years	Body Weight, kg	Healthy (H) Participants or Patients With AD	Diabetic (D) or Nondiabetic (N)	Plasma Glucose, mg/dL	Plasma Zinc, μg/mL[a]	Plasma Copper, μg/mL	Urine Zinc, μg/L	STMS	MMSE
1	F	64	66	H	N	76	0.82	1.31	126[b]	38/38	
2	M	88	62	AD	D	129[c]	0.81	0.93	1384[b]	21/38[d]	NA
3	M	63	89	H	N	89	0.84	1.06	169[b]	35/35	
4	M	63	88	AD	N	81	0.86	0.94	108[b]	27/38	24
5	M	69	73	H	N	74	0.88	1.14	377	32/38	
6	M	78	77	AD	N	92	0.70	0.89	106[b]	8/38	10
7	F	62	56	H	N	87	0.78	1.06	33[b]	36/38	
8	F	55	105	H	N	90	0.96	1.22	409	37/38	
9	F	70	70	AD	D	181[c]	0.92	1.34	872[b]	25/38	21
10	F	76	53	AD	N	85	0.70	1.05	42[b]	24/38	19
11	F	77	64	H	N	84	0.66	1.05	225[b]	37/38	
12	F	74	71	AD	N	97	0.75	1.46[e]	346	22/38	16

Abbreviations: AD, Alzheimer disease; F, female; M, male; MMSE, Mini-Mental State Examination; NA, not available; STMS, Short Test of Mental Status; SUV, standardized uptake value.
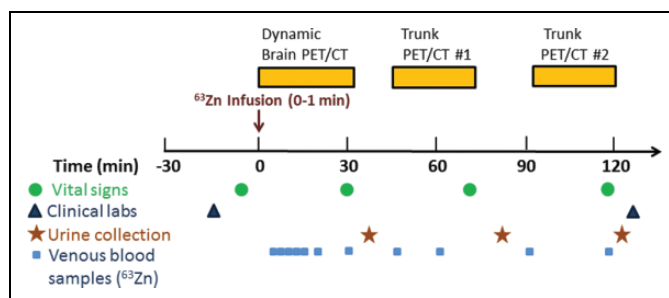[a]All plasma zinc levels were within the normal range (0.66-1.1 μg/mL).
[b]Urine zinc levels outside the normal range (300-600 μg/L).
[c]Fasting plasma glucose outside the normal range (70-100 mg/dL).
[d]Last STMS performed 3 years prior.
[e]Plasma copper level above the normal range (0.75-1.45 μg/mL).

Figure 1. Experimental protocol.

Positron Emission Tomography Image Analysis

Magnetic resonance imaging (MRI; 3 T) and PET/CT scans using ^{11}C-PiB were acquired and analyzed as described in detail elsewhere.[13] The [63]Zn-PET/CT and MR images were transferred to a workstation running PMOD (version 3.5, Fusion Toolbox; PMOD Technologies, Zurich, Switzerland) for analysis. The CT images for [63]Zn-zinc citrate were registered to the patient's MR images using a rigid transformation based on normalized mutual information. The same transformation was applied to the dynamic [63]Zn-PET series. In the case of the whole-body series, only those [63]Zn-PET and CT slices that contain the head were registered to the MRI. Next, the participant's MRI was spatially normalized to an MRI template using a nonlinear warping procedure. The template was a T1-weighted MRI data set having 91×109 matrix with 91 slices and 2 mm^3 voxels.[14] The same transformation was then applied to all PET series. A predefined atlas of volumes of interest (VOIs) was defined for the template. The atlas of VOIs was subsequently superimposed on the PET images and time–activity curves (TACs) were generated. The uptake from the whole-body data was incorporated into the TACs from the dynamic data. An "AD-global" VOI was created by inclusion of VOIs that have importance in AD (cingulate, precuneus, anterior cingulate, parietal lobe, prefrontal, temporal, pre- and postcentral regions). ^{11}C-PiB-PET cortical uptake was normalized to cerebellar gray matter to obtain the standardized uptake value ratio (SUVR). All patients with AD showed amyloid-β-positive SUVR >1.5 for the AD-global VOI. All healthy participants showed amyloid-β-negative SUVR <1.5 for the AD-global VOI.

Safety Measurements for [63]Zn-Zinc Citrate Administration

Vital signs (heart rate, systolic and diastolic blood pressures, respiratory rate, temperature) were measured prior to [63]Zn-zinc citrate administration and at 30, 70, and 115 minutes PI. Venous blood samples were taken prior to [63]Zn-zinc citrate administration and at ∼130 minutes PI for a panel of clinical laboratory tests to evaluate the safety of the radiotracer administration.

Pharmacokinetics of [63]Zn-Zinc Citrate in Venous Blood Samples

Peak time was defined as the time of maximum measurement (minimum of $t > 1$ minute) with maximum observed concentration. Half-clearance times were defined as the time from peak concentration to an estimated 50% of peak concentration. Concentrations were modeled for each individual for whole-blood and plasma separately using the γ distribution, with time $t = 0$ defined as the time at peak for each participant. Plateau was defined as the first interval of time starting after $t = 20$ minutes with an observed change in concentration less than 0.05/minute. Time to plateau was defined as the end point of the interval

in which plateau had occurred in both whole blood and plasma. Between-group comparisons of pharmacokinetic characteristics were performed using Wilcoxon rank sum tests.

Statistical Analysis

Summary statistics are shown as mean $\pm$ standard deviation (SD) for continuous variables and N (%) for categorical variables. Participants were divided into 2 groups: normal, healthy adults and patients with AD based on the characteristics described in Human Participants section. Between-group comparisons for baseline demographics and clinical characteristics used Wilcoxon rank sum test or Fisher exact test for continuous and categorical variables, respectively. Between-group comparisons for ^{63}Zn-zinc citrate, %dose/organ, ^{11}C-PiB, and ^{18}F-FDG were performed using Wilcoxon rank sum tests. Due to the limited power to include multiple main effects in 1 model, for comparisons either between preinjection and PI characteristics (with the exception of vital signs) or between PET scans, results are presented in 2 ways: first, a between-time comparison was performed using Wilcoxon signed rank tests; second, differences in the amount of change between groups was assessed using Wilcoxon rank sum tests. For ^{11}C-PiB, regional cerebral uptake was normalized to cerebellar uptake. For ^{18}F-FDG, regional cerebral uptake was normalized to pons uptake. Vital signs (heart rate, temperature, respiratory rate, systolic and diastolic blood pressures) were taken once preinjection and 3 times PI and were compared using Kruskal-Wallis rank sum tests. Reported P values have not been corrected for multiple testing. All Wilcoxon tests were exact, 2-sided tests. Statistical analysis was performed using R (version 3.1.1; Vienna, Austria).

Results

Participant Characteristics

The participant characteristics are shown in Table 1. All participants showed plasma zinc concentrations in the normal range of 0.66 to 1.1 μg/mL. Two of 6 patients with AD were diabetic (participants 2 and 9). Both of the diabetic patients with AD showed abnormally high plasma glucose and urinary zinc (>600 μg/L) concentrations, the latter being consistent with the previous reports of hyperzincuria in type 2 diabetics in the absence of neurodegeneration.[15,16] Nevertheless, the plasma zinc levels in these 2 participants were in the normal range. The majority of nondiabetic participants showed abnormally low concentrations of zinc in urine (<300 μg/L), possibly due to their fasting state and heavy consumption of water in the morning of the study as instructed. One healthy elderly participant (data not shown) was excluded post hoc from the study because of an abnormally low fasting plasma zinc concentration indicative of a state of zinc depletion.

Safety Measurements for ^{63}Zn-Zinc Citrate Administration

Measurements of vital signs (heart rate, systolic and diastolic blood pressures, respiratory rate, temperature) and a comprehensive panel of clinical laboratory tests for the assessment of radiopharmaceutical safety are reported in Supplemental Information. These tests showed the ^{63}Zn-zinc citrate administration to be well tolerated with very few results outside the normal range and no pattern indicative of an effect of radiotracer administration across participants. There was not sufficient evidence to conclude that a difference exists between the experimental groups nor that the vitals at any time point were different than another; all P values were >0.2, with the exception of between-group comparison at baseline respiratory rate ($P = 0.138$).

Pharmacokinetics of ^{63}Zn-Zinc Citrate in Venous Blood

Figure 2 shows representative curves for venous whole–blood and plasma concentrations of ^{63}Zn radioactivity following intravenous administration of ^{63}Zn-zinc citrate. The pharmacokinetic properties are summarized in Table 2. Peak concentration of ^{63}Zn in venous plasma and in whole blood occurred within 10 minutes. The ratio of concentrations of ^{63}Zn in whole blood to plasma increased over time to a plateau value of 0.878 ± 0.117 in the healthy group and 0.869 ± 0.138 in the AD group at 1 hour, evidencing the transport of ^{63}Zn from plasma to erythrocytes. Some transport into erythrocytes may have occurred after samples were withdrawn from the participants, although the samples were placed immediately on ice to slow down this process. Plasma half-clearance times were approximately 8 minutes (healthy: 7.06 ± 2.19, AD: 8.39 ± 1.61). There were no statistically significant differences in the pharmacokinetic parameters for patients with AD versus healthy participants.

Biodistribution of ^{63}Zn-Zinc Citrate

Figure 3 shows PET/CT images of ^{63}Zn-zinc citrate in representative participants. Prominent uptake was observed in the liver, with pancreas, kidneys, spleen, and intestines showing moderate levels of uptake. Intestinal uptake was consistent across duodenum, jejunum, and ileum (Figure 4). This suggests that intestinal uptake of ^{63}Zn resulted from the transport of radiotracer from blood, not only the possible secretion into the upper small bowel by liver, pancreas, or gallbladder. Brain uptake was low but apparent on images. No qualitative differences were observed in the PET images of whole-body distribution of ^{63}Zn-zinc citrate in patients with AD relative to healthy participants. Also, no qualitative differences could be seen in the images from the last trunk PET/CT study at 95 to 120 minutes in comparison with the images acquired at 45 to 70 minutes.

Table 3 shows the biodistribution (standardized uptake values [SUVs]) for ^{63}Zn-zinc citrate obtained from head to thigh PET/CT images acquired at 45 to 70 minutes and 95 to 120 minutes PI. Earlier uptake data are reported in Table S1. Tissues with the highest uptake were liver, pancreas, and kidney. The whole-organ uptakes in liver and pancreas were 51.2% $\pm$ 5.5% and 1.07% $\pm$ 0.60%, respectively, across all participants, and these values were not statistically different for patients with AD relative to healthy participants. Thus, hepatic
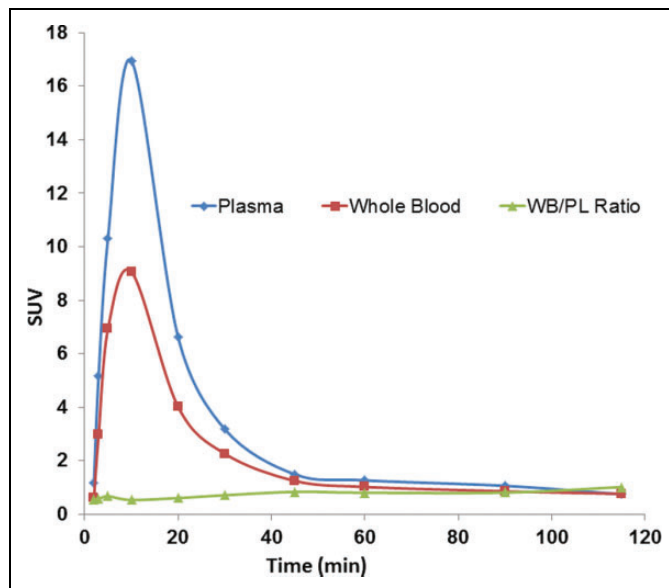
Figure 2. Representative kinetics of ^{63}Zn radioactivity in venous whole blood and plasma of healthy participant. The ratio of concentrations of ^{63}Zn in whole blood to plasma increased over time, evidencing transport of ^{63}Zn from plasma to erythrocytes.

**Table 2.** Pharmacokinetic Properties of ^{63}Zn-Zinc Citrate.[a]

Property	Healthy Participants	Patients With AD
Time of peak, plasma, minutes	8.25 ± 2.87	7.60 ± 2.51
Peak concentration, plasma (SUV)	11.00 ± 5.44	10.93 ± 2.50
Half-clearance time, plasma, minutes	7.06 ± 2.19	8.39 ± 1.61
Time of peak, whole blood, minutes	9.50 ± 0.58	6.90 ± 2.61
Peak concentration, whole blood (SUV)	6.52 ± 2.27	7.04 ± 1.20
Half-clearance time, whole blood, minutes	9.078 ± 1.93	10.35 ± 2.51
WB:plasma ratio at plateau	0.878 ± 0.117	0.869 ± 0.138
Time of ratio plateau, minutes	56.25 ± 7.5	57.00 ± 6.71

Abbreviations: AD, Alzheimer disease; SUV, standardized uptake value; WB, whole blood.
[a]No statistically significant differences were found on comparing AD and healthy groups.

uptake of intravenously administered ^{63}Zn-zinc citrate was hugely predominant and clearance of ^{63}Zn by the liver was negligible between the first and second trunk PET scans. Moderate uptake was seen in pituitary, salivary glands, thyroid, spleen, stomach, intestines, prostate (in males), and bone marrow. Moderately low uptake was found across brain regions with SUVs ranging 0.3 to 0.5. This level of uptake in brain regions could not be explained by ^{63}Zn radioactivity in blood vessels of the brain as it was much higher (SUV ~ 0.4, Table 3) than the product of blood volume (~5%) and whole-blood concentration (SUV ~ 1, Figure 3). Urinary excretion of ^{63}Zn was very minimal at 2 hours and similar for the 2 participant groups (healthy 0.041% ± 0.020%; AD 0.047% ± 0.052%).
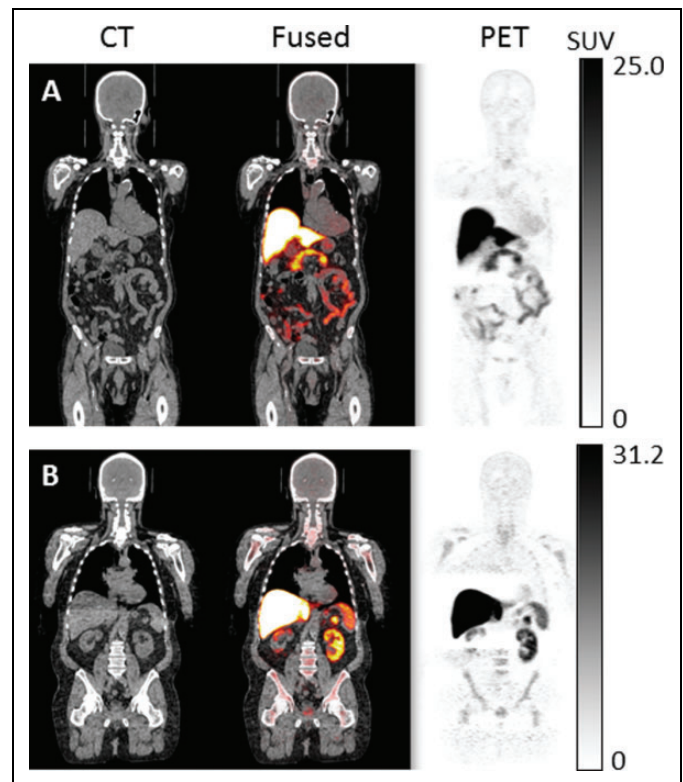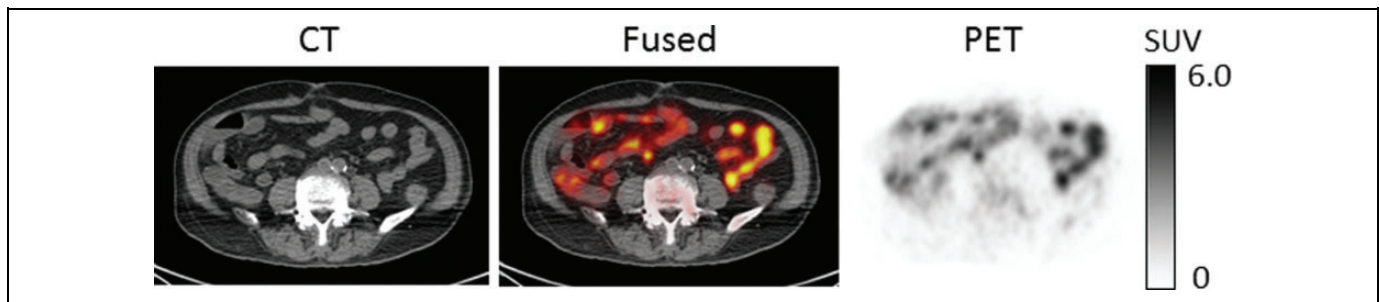

Figure 3. Positron emission tomography (PET)/computed tomography (CT) images in representative patient with Alzheimer disease (AD; A) and healthy elderly participant (B) at 45 to 70 minutes post-administration of ^{63}Zn-zinc citrate. Hepatic uptake is largely prominent, while lower uptake by pancreas, spleen, kidneys and intestines, bone marrow, and brain was observed. No qualitative differences were observed in the PET images of whole-body distribution of ^{63}Zn-zinc citrate in patients with AD relative to healthy participants.

The 2 diabetic patients with AD showed the highest urinary excretions (0.133% and 0.086%), consistent with hyperzincuria in these participants.

Brain Kinetics of ^{63}Zn-Zinc Citrate

A 30-minute dynamic PET acquisition was commenced over the brain at the beginning of the ^{63}Zn-zinc citrate administration. In addition to these early data, the cerebral regions in the 2 later trunk PET/CT scans were available for completing the regional ^{63}Zn TACs out to 2 hours. Atlas-based cerebral regions were defined on the MRI images obtained for each participant and then transferred for quantitative region-of-interest evaluation on the PET images, as illustrated in Figure 5A. As mentioned previously, the absolute uptake data did not shown any differences between AD and healthy experimental groups (Table 3). However, clearance kinetics over the period 27.5 to 97.5 minutes in several regions were significantly slower in patients with AD relative to healthy participants (Figures 5B and 6). To provide quantitative indices of clearance rate, we evaluated the percentage changes in SUV exhibited within the brain regions between various time points.

Figure 4. Abdominal positron emission tomography (PET)/computed tomography (CT) images of [63]Zn-zinc citrate distribution acquired 45 to 70 minute postinjection (PI) show intraluminal distribution in intestines.

Table 3. Biodistribution (SUV) of [63]Zn-Zinc Citrate in Healthy Elderly Participants and Patients With AD.[a]

| Tissue	PET Scan at 45-70 Minutes		PET Scan at 95-120 Minutes	
	Healthy	Patients With AD	Healthy	Patients With AD
AD-global	0.39 ± 0.05	0.37 ± 0.07	0.35 ± 0.05	0.35 ± 0.06
Parietal	0.36 ± 0.05	0.34 ± 0.06	0.33 ± 0.04	0.33 ± 0.06
Cingulate, precuneus	0.41 ± 0.05	0.38 ± 0.06	0.37 ± 0.05	0.37 ± 0.05
Prefrontal cortex	0.37 ± 0.05	0.36 ± 0.07	0.33 ± 0.05	0.33 ± 0.06
Orbitofrontal	0.39 ± 0.06	0.36 ± 0.06	0.32 ± 0.06	0.33 ± 0.08
Lateral temporal	0.39 ± 0.05	0.37 ± 0.08	0.35 ± 0.05	0.34 ± 0.07
Primary visual cortex	0.50 ± 0.06	0.46 ± 0.09	0.44 ± 0.06	0.44 ± 0.08
Cerebellum	0.46 ± 0.05	0.46 ± 0.09	0.41 ± 0.06	0.41 ± 0.08
Anterior cingulate	0.34 ± 0.05	0.31 ± 0.06	0.30 ± 0.05	0.28 ± 0.05
Occipital cortex	0.44 ± 0.05	0.41 ± 0.08	0.40 ± 0.05	0.40 ± 0.07
Medial temporal	0.39 ± 0.06	0.36 ± 0.06	0.35 ± 0.07	0.33 ± 0.04
Pons	0.45 ± 0.08	0.42 ± 0.09	0.36 ± 0.05	0.38 ± 0.09
Pituitary	3.00 ± 0.48	2.78 ± 0.65	2.61 ± 0.42	2.65 ± 0.261
Parotid gland	2.56 ± 1.10	2.43 ± 0.42	2.47 ± 0.92	2.64 ± 0.55
Submandibular gland	3.17 ± 0.67	3.14 ± 0.51	3.32 ± 0.62	3.12 ± 0.68
Thyroid	3.94 ± 1.01	4.15 ± 1.93	4.17 ± 1.05	4.26 ± 1.70
Lung	0.27 ± 0.12	0.30 ± 0.15	0.30 ± 0.09	0.31 ± 0.11
Heart	0.81 ± 0.22	1.10 ± 0.17	0.76 ± 0.21	1.17 ± 0.14
Breast (females)	0.04 ± 0.04	0.09 ± 0.12	0.05 ± 0.06	0.10 ± 0.11
Liver	33.2 ± 3.1	30.6 ± 7.5	34.3 ± 5.0	31.3 ± 7.9
Spleen	4.46 ± 0.60	5.00 ± 0.70	4.12 ± 0.71	4.85 ± 0.48
Pancreas	12.1 ± 4.0	13.0 ± 3.8	13.5 ± 3.4	12.4 ± 2.9
Stomach	4.34 ± 1.08	3.96 ± 0.87	4.68 ± 0.88	5.07 ± 1.07
Ileum	5.66 ± 1.13	4.68 ± 0.41	5.47 ± 1.56	4.77 ± 1.89
Kidney	9.94 ± 1.02	10.72 ± 1.69	10.09 ± 1.30	10.80 ± 1.79
Prostate (males)	3.15 ± 0.04	3.14 ± 2.07	3.90 ± 0.52	3.67 ± 3.02
Testicles (males)	0.57 ± 0.36	0.70 ± 0.27	0.42 ± 0.08	0.62 ± 0.02
Bone	0.24 ± 0.10	0.21 ± 0.11	0.24 ± 0.24	0.25 ± 0.12
Bone marrow	1.41 ± 0.20	1.40 ± 0.31	1.42 ± 0.47	1.50 ± 0.54
Skeletal muscle	0.17 ± 0.03	0.16 ± 0.06	0.16 ± 0.02	0.18 ± 0.04

Abbreviations: AD, Alzheimer disease; PET, positron emission tomography; SUV, standardized uptake value.
[a]No statistically significant differences were found on comparing AD and healthy groups at these time points.

Standardized uptake value changes were significantly smaller in patients with AD for the following regions: AD global region, left parietal lobe, left prefrontal cortex, left lateral temporal lobe, orbitofrontal cortex, and occipital cortex ($P < 0.05$). All of these regions were also characterized by ^{11}C-PiB accumulation indicative of amyloid-β plaque. Regional cerebral [63]Zn clearance values from 47.5 to 92.5 minutes are shown in Figure 7 in relationship with SUVRs for ^{11}C-PiB and ^{18}F-FDG in the same regions. Again, [63]Zn clearance was lower in patients with AD in several regions correlating with abnormalities on the ^{11}C-PiB and ^{18}F-FDG scans, although variability in [63]Zn clearance values were relatively larger. On the other hand, several regions not typically associated with ^{11}C-PiB positive uptake (medial temporal, cerebellum, and pons) did not show statistically significant [63]Zn SUV changes between the AD and healthy groups.
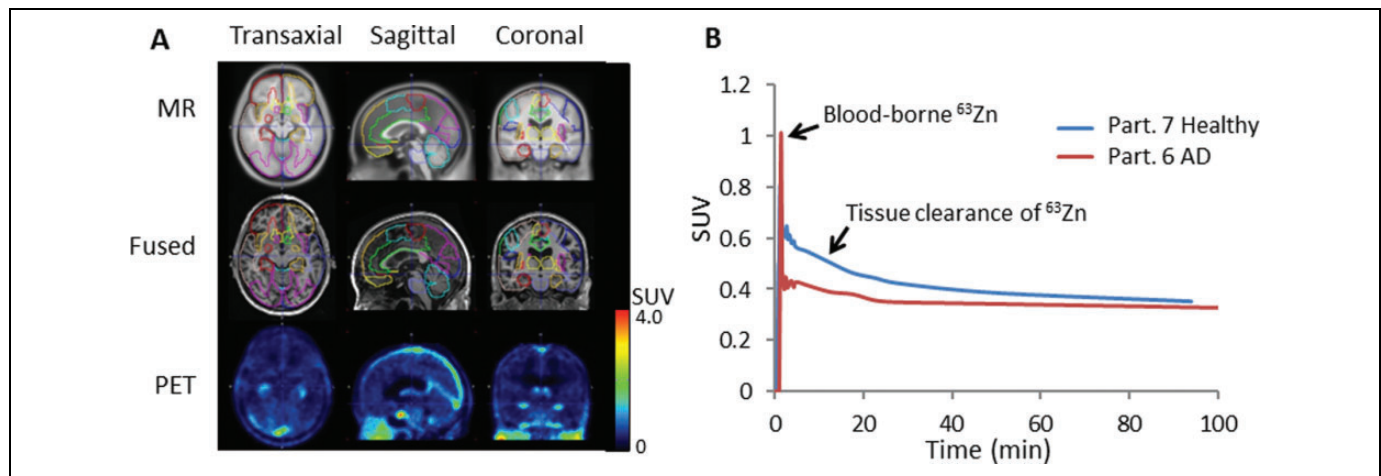
Figure 5. A, Regional image analysis of brain kinetics of [63]Zn-zinc citrate. T1-weighted magnetic resonance (MR) images are shown at top and coregistered [63]Zn-PET images at 45 to 50 minutes postinjection (PI) are shown at the bottom. Outlines of volumes of interest (VOIs) are shown in various colors on the MR and fused images. Low levels of zinc uptake (SUV < 0.5) were observed across brain. B, Representative left prefrontal cortex time–activity curves in patients with AD and healthy participants.
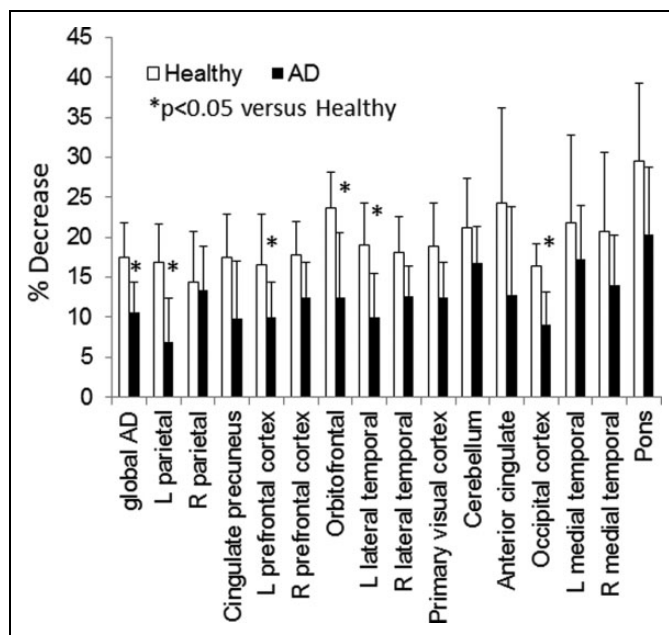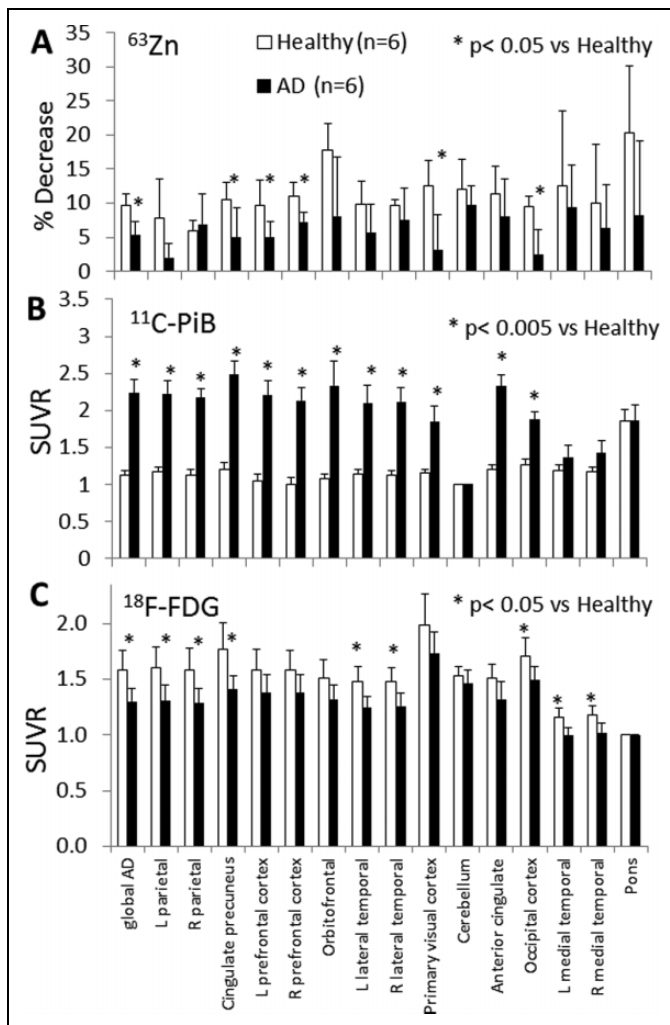

Figure 6. Regional cerebral clearances of [63]Zn between 27.5 and 92.5 minutes postinjection (PI).

Discussion

This first-in-human PET imaging study of zinc distribution after intravenous administration of [63]Zn-zinc citrate was aimed at answering 2 primary questions. First, what are the major tissues that take up zinc and what potential clinical role might [63]Zn-PET play in these tissues? Second, can [63]Zn-PET be useful to evaluate the uptake and turnover of zinc in brains of patients with AD? The answer to the first question was predominantly liver, with moderately high uptake of zinc in the pancreas, kidney, and GI tract. Since zinc homeostasis critically depends on the balance of intake from diet and excretion (primarily through the gut), it was not surprising to find the locus of initial distribution of [63]Zn in organs of the digestive system, including liver and pancreas. The findings that more than half of the injected dose was found to be taken up by liver and hepatic [63]Zn concentration was stable up to at least 2 hours PI underscore the importance of liver for storage and redistribution of zinc. Zinc deficiency is well documented in a variety of liver diseases.[17] Disturbances of zinc homeostasis are associated with hepatitis B infection,[18] cirrhosis,[19] alcoholic liver disease,[20] nonalcoholic fatty liver disease,[21] hepatocellular carcinoma,[22] and malabsorption.[23] Subnormal hepatic zinc content is a common finding in these disease states. Thus, PET imaging of hepatic zinc kinetics using [63]Zn as probe may play a role in evaluating a variety of diseases that affect the liver. The pancreas also showed high and persistent uptake of [63]Zn-zinc citrate in this study. Zinc plays an important role in a variety of pancreatic and β-cell functions, including insulin storage and secretion[24] and secretion of zinc-associated pancreatic enzymes into the duodenum.[25] Indeed, zinc homeostasis suffers in diseases of the pancreas, including chronic pancreatitis[26] and diabetes.[24] The pancreas was readily imaged by [63]Zn-PET, although differentiation of β-cell uptake from acinar pancreatic uptake would be precluded by the very small β-cell volume fraction. Renal uptake of [63]Zn-zinc citrate was also high and undiminished from the first and second trunk PET scans. The urinary excretion of [63]Zn radioactivity was found to be minimal (<0.1%), consistent with the known fate of zinc in the kidney to be uptaken by epithelial cells of the renal tubular system.[27] The moderate uptake of [63]Zn-zinc citrate across the small intestine supports the important role of zinc in digestion. The finding of [63]Zn radioactivity in the lumen of the ileum (Figure 4) as early as an hour (the earliest image of the abdomen) after intravenous administration argues that intestinal absorption of zinc is significant and may provide zinc as an essential nutrient to intestinal microbiota. Evidence has been found for high-affinity zinc transporters in several bacterial species that populate within the intestines,[28] which could explain the high luminal

Figure 7. A, Regional cerebral clearances of ^{63}Zn between 47.5 and 92.5 minutes postinjection (PI). B, Standardized uptake value ratios (SUVRs) for ^{11}C-PiB normalized to the cerebellum. C, The SUVRs for ^{18}F-FDG normalized to the pons.

accumulation of ^{63}Zn. This finding underscores the importance of the rapid exchange of zinc between blood and small intestine relevant to overall zinc homeostasis and the ability of ^{63}Zn-PET to provide noninvasive assessment of this exchange. It is possible that ^{63}Zn-PET could provide a new tool to evaluate intestinal zinc dynamics in patients presenting with zinc deficiency, for example, patients with Crohn's disease[29] and inflammatory bowel disease.[30]

The second (and primary) aim of this study was to obtain data on zinc uptake and turnover in the brains of patients with AD. Since zinc is known to bind with high affinity to amyloid-β protein[31] and be an essential component of amyloid β-protein aggregates in AD brains,[32] we postulated that ^{63}Zn kinetics after intravenous administration of ^{63}Zn-zinc citrate might be different in amyloid-β plaque-rich regions in AD brains in comparison with the same regions in healthy elderly participants. This study recruited elderly patients already enrolled in an ongoing multiyear longitudinal imaging study within the

Mayo Clinic Alzheimer's Research Center utilizing MR, FDG-PET, and ^{11}C-PiB-PET. ^{11}C-PiB-PET has been extensively validated as a PET probe of regional cerebral amyloid-β plaque burden in aging brain and AD.[33] Transport of ^{63}Zn-zinc citrate across the BBB into the brain was evidenced by SUVs of around 0.5 following the vascular washout phase in the first 4 to 7 minutes postadministration (Figure 5B). Measurements of the initial uptake into brain regions at 12.5 minutes PI did not show regional variation and were not statistically different in patients with AD compared to healthy participants. However, ^{63}Zn clearance rates from brain regions did show statistically significant differences with respect to brain region and the experimental group. Slower ^{63}Zn clearance rates were found in patients with AD in the following regions (Figure 6, $P < .05$): AD global (comprised of cingulate, precuneus, anterior cingulate, left and right parietal lobes, left and right prefrontal cortices, left and right temporal lobes, and pre- and postcentral regions), cingulate, precuneus, left and right prefrontal cortices, left parietal, left lateral temporal, orbitofrontal cortex, primary visual cortex, and occipital cortex. The brain regions comprising the "AD global" region are all regions that typically show elevated ^{11}C-PiB-PET accumulation in patients with AD. Slower ^{63}Zn clearance may result from enhanced binding of ^{63}Zn-zinc in cerebral tissue, possibly to AD-related protein aggregates. In addition to the well-established binding properties of zinc to amyloid-β plaque, there is recent evidence that zinc also binds to tau protein, another protein that accumulates in AD brains in aggregate form and is strongly implicated in the pathophysiology of AD.[34] Furthermore, there are elevated levels of soluble oligomers of amyloid-β in AD brain that could also represent binding sites for intracerebral zinc.[35]

Given the evidence that there is a slowing of ^{63}Zn-zinc clearance from certain regions of the brain in patients with AD, there is potential that this measurement could serve as a noninvasive indication of zinc dyshomeostasis in the AD brain. Larger and more diverse study populations will be needed to establish the clinical potential of this technique for the evaluation of neuronal pathology. Also, the mechanistic basis for regional differences in ^{63}Zn clearance rate has yet to be determined. As PET imaging agents of tau protein aggregates become more available, it will be of interest to correlate ^{63}Zn kinetics with both amyloid-β and tau pathology. It will also be important to look at factors other than aberrant protein accumulations in brain that could affect intracerebral zinc turnover, such as zinc deficiency. Indeed, 1 mentally healthy participant (82 years) was excluded from analysis in this study on the basis of a subnormal plasma zinc concentration indicative of zinc deficiency. The ^{63}Zn clearance rates across all brain regions for this participant were markedly lower than others in the healthy group (data not shown) consistent with the notion that brain kinetics of zinc may be abnormal in elderly participants who are in a zinc-deficient state.[36]

Several study limitations should be noted. Arterial input functions were not obtained that may allow investigation of more sophisticated models to regress the cerebral ^{63}Zn TACs.

Kinetic rate constants for blood–tissue and tissue–blood transport of ^{63}Zn could not be assessed in this study. Clearance rates of ^{63}Zn from tissue at later times were inferred from changes in SUV. Future work should employ arterial input functions to provide more meaningful quantitative indices of ^{63}Zn kinetics in the brain. Another limitation of the study was the small size of the experimental groups (n = 6 each) and the limited selection of clinically diagnosed patients with AD that showed positive ^{11}C-PiB scans and hypometabolism on FDG-PET scans. Future work is warranted in larger participant groups and inclusion of participants who have a range of cognitive impairment. Effects of potential perfusion changes in AD brain were not assessed in this study. Decreased perfusion in AD-relevant brain regions could be an alternative explanation for the slower clearance rate of ^{63}Zn, although the lack of abnormality seen in the early uptake of ^{63}Zn in the same regions would argue against a perfusion effect. The average age of the AD group (75 years) was greater than that of the healthy group (65 years), although not statistically significant ($P = 0.06$). The AD cohort included 2 participants who were diabetic. Since zinc dyshomeostasis has been noted in diabetics,[15,16] this may represent a potential confound. However, the plasma zinc levels in the 2 diabetic patients were in the normal range, and separate analysis of ^{63}Zn clearance rates with the diabetic patients being removed showed similar discrepancies to the healthy group. Finally, the level of signal in the brain is low, reflecting the transport limitation on zinc into the brain imposed by the BBB. Although the inclusion of a brain-penetrant zinc ionophore in the ^{63}Zn formulation could potentially bring more ^{63}Zn radioactivity into the brain, the use of such a carrier could alter the natural binding processes within the brain and increase the risk of adverse events. Future investigations (in preclinical models) with zinc-binding ionophores as carriers for ^{63}Zn are anticipated. Should the ^{63}Zn-PET scans show sensitivity to changes in cerebral zinc transport resulting from ionophore administration, this may be developed into a useful tool for monitoring ionophore therapies.

Conclusion

A first-in-human PET imaging study of ^{63}Zn-zinc citrate was performed in patients with AD and healthy elderly participants. Prominent uptake of ^{63}Zn radioactivity was seen in the liver ($\sim 51\%$ dose/organ), pancreas, kidney, and GI tract. Brain uptake was relatively low (SUVs ~ 0.4) but sufficient to allow assessment of ^{63}Zn uptake and clearance patterns on a regional basis. Although brain uptake was consistent across brain regions and experimental groups, slower clearance rates of ^{63}Zn radioactivity were seen in several brain regions in patients with AD relative to healthy participants. The regions with slower ^{63}Zn clearance corresponded to regions of known amyloid-β pathology on ^{11}C-PIB-PET scans and lower uptake on FDG-PET scans. Positron emission tomography imaging with ^{63}Zn-zinc citrate represents a new tool for noninvasive assessment of zinc dynamics in the living human body.

References

1. Frassinetti S, Bronzetti G, Caltavuturo L, Cini M, Croce CD. The role of zinc in life: a review. *J Environ Pathol Toxicol Oncol*. 2006;25(3):597-610. doi:10.1615/JEnvironPatholToxicolOncol.v25.i3.40.

2. Penny ME. Zinc supplementation in public health. *Ann Nutr Metab*. 2013;62(suppl 1):31-42. doi:10.1159/000348263.

3. Miao X, Sun W, Fu Y, Miao L, Cai L. Zinc homeostasis in the metabolic syndrome and diabetes. *Front Med*. 2013;7(1):31-52. doi:10.1007/s11684-013-0251-9.

4. Costello LC, Levy BA, Desouki MM, et al. Decreased zinc and downregulation of ZIP3 zinc uptake transporter in the development of pancreatic adenocarcinoma. *Cancer Biol Ther*. 2011; 12(4):297-303. doi:10.4161/cbt.12.4.16356.

5. Kolenko V, Teper E, Kutikov A, Uzzo R. Zinc and zinc transporters in prostate carcinogenesis. *Nat Rev Urol*. 2013;10(4): 219-226. doi:10.1038/nrurol.2013.43.

6. Alam S, Kelleher SL. Cellular mechanisms of zinc dysregulation: a perspective on zinc homeostasis as an etiological factor in the development and progression of breast cancer. *Nutrients*. 2012; 4(8):875-903. doi:10.3390/nu4080875.

7. Craddock TJ, Tuszynski JA, Chopra D, et al. The zinc dyshomeostasis hypothesis of Alzheimer's disease. *PLoS One*. 2012; 7(3):e33552. doi:10.1371/journal.pone.0033552

8. Lannfelt L, Blennow K, Zetterberg H, et al; PBT2-201-EURO study group. Safety, efficacy, and biomarker findings of PBT2 in targeting Abeta as a modifying therapy for Alzheimer's disease: a phase IIa, double-blind, randomised, placebo-controlled trial. *Lancet Neurol*. 2008;7(9):779-786. doi:10.1016/S1474-4422(08)70167-4.

9. Bredesen DE. Metabolic profiling distinguishes three subtypes of Alzheimer's disease. *Aging (Albany NY)*. 2015;7(8):595-600.

10. Liang SH, Holland JP, Stephenson NA, et al. PET neuroimaging studies of [^{18}F]CABS13 in a double transgenic mouse model of Alzheimer's disease and nonhuman primates. *ACS Chem Neurosci*. 2015;6(4):535-541. doi:10.1021/acschemneuro.5b00055.

11. Bush AI, Tanzi RE. Therapeutics for Alzheimer's disease based on the metal hypothesis. *Neurotherapeutics*. 2008;5(3):421-432. doi:10.1016/j.nurt.2008.05.001.

12. DeGrado TR, Pandey MK, Byrne JF, et al. Preparation and preliminary evaluation of^{63}Zn-zinc citrate as a novel PET imaging biomarker for zinc. *J Nucl Med*. 2014;55(8):1348-1354. doi:10.2967/jnumed.114.141218.

13. Lowe VJ, Kemp BJ, Jack CR Jr, et al. Comparison of ^{18}F-FDG and PiB PET in cognitive impairment. *J Nucl Med*. 2009;50(6): 878-886. doi:10.2967/jnumed.108.058529.

14. Vemuri P, Gunter JL, Senjem ML, et al. Alzheimer's disease diagnosis in individual subjects using structural MR images: validation studies. *Neuroimage*. 2008;39(3):1186-1197. doi:10.1016/j.neuroimage.2007.09.073.

15. Kinlaw WB, Levine AS, Morley JE, Silvis SE, McClain CJ. Abnormal zinc metabolism in type II diabetes mellitus. *Am J Med*. 1983;75(2):273-277. doi:10.1016/0002-9343(83)91205-6.

16. Xu J, Zhou Q, Liu G, Tan Y, Cai L. Analysis of serum and urinal copper and zinc in Chinese Northeast population with the prediabetes or diabetes with and without complications. *Oxid Med Cell Longev*. 2013;2013:635214. doi:10.1155/2013/635214.

17. Kahn AM, Helwig HL, Redeker AG, Reynolds TB. Urine and serum zinc abnormalities in disease of the liver. *Am J Clin Pathol*. 1965;44(4):426-435.

18. Gür G, Bayraktar Y, Özer D, Özdogan M, Kayhan B. Determination of hepatic zinc content in chronic liver disease due to hepatitis B virus. *Hepatoqastroenterology*. 1998;45(20): 472-476.

19. Poo JL, Romero R, Rodriguez F, et al. Serum zinc concentrations in two cohorts of 153 healthy subjects and 100 cirrhotic patients from Mexico City. *Dig Dis*. 1995;13(2):136-142.

20. Bode CJ, Hanisch P, Henning H, Koenig W, Richter FW, Bode C. Hepatic zinc content in patients with various stages of alcoholic liver disease and in patients with chronic active and chronic persistent hepatitis. *Hepatology*. 1988;8(6):1605-1609.

21. Guo CH, Chen PC, Ko WS. Status of essential trace minerals and oxidative stress in viral hepatitis C patients with nonalcoholic fatty liver disease. *Int J Med Sci*. 2013;10(6):730-737. doi:10.7150/ijms.6104.

22. Franklin RB, Levy BA, Zou J, et al. ZIP14 zinc transporter downregulation and zinc depletion in the development and progression of hepatocellular cancer. *J Gastrointest Cancer*. 2012;43(2): 249-257. doi:10.1007/s12029-011-9269-x.

23. Walker BE, Dawson JB, Kelleher J, Lasowsky MS. Plasma and urinary zinc in patients with malabsorption syndromes or hepatic cirrhosis. *Gut*. 1973;14(12):943-948.

24. Li YV. Zinc and insulin in pancreatic beta-cells. *Endocrine*. 2014; 45(2):178-189. doi:10.1007/s12020-013-0032-x.

25. Gjørup I, Petronijevic L, Rubinstein E, Andersen B, Worning H, Burcharth F. Pancreatic secretion of zinc and copper in normal subjects and in patients with chronic pancreatitis. *Digestion*. 1991;49(3):161-166.

26. Rajesh G, Girish BN, Vaidyanathan K, Balakrishnan V. Diet, nutrient deficiency and chronic pancreatitis. *Trop Gastroenterol*. 2013;34(2):68-73.

27. Kumar R, Prasad R. Functional characterization of purified zinc transporter from renal brush border membrane of rat. *Biochim Biophys Acta*. 2000;1509(1-2):429-439. doi:10.1016/S0005-2736(00)00325-4.

28. Gielda LM, DiRita VJ. Zinc competition among the intestinal microbiota. *MBio*. 2012;3(4):e00171-12. doi:10.1128/mBio.00171-12.

29. Brignola C, Belloli C, De Simone G, et al. Zinc supplementation restores plasma concentrations of zinc and thymulin in patients with Crohn's disease. *Aliment Pharmacol Ther*. 1993;7(3):275-280.

30. Alkhouri RH, Hashmi H, Baker RD, Gelfond D, Baker SS. Vitamin and mineral status in patients with inflammatory bowel disease. *J Pediatr Gastroenterol Nutr*. 2013;56(1):89-92. doi:10.1097/MPG.0b013e31826a105d.

31. Bush AI, Pettingell WH, Multhaup G, et al. Rapid induction of Alzheimer A beta amyloid formation by zinc. *Science*. 1994; 265(5177):1464-1467.

32. Religa D, Strozyk D, Cherny RA, et al. Elevated cortical zinc in Alzheimer disease. *Neurology*. 2006;67(1):69-75.

33. Driscoll I, Troncoso JC, Rudow G, et al. Correspondence between in vivo ^{11}C-PiB-PET amyloid imaging and postmortem, regionmatched assessment of plaques. *Acta Neuropathol*. 2012;124(6): 823-831. doi:10.1007/s00401-012-1025-1.

34. Huang Y, Wu Z, Cao Y, Lang M, Lu B, Zhou B. Zinc binding directly regulates tau toxicity independent of tau hyperphosphorylation. *Cell Rep*. 2014;8(3):831-842. doi:10.1016/j.celrep.2014.06.047.

35. Selkow DJ, Masters CL. Biochemistry of amyloid β-protein and amyloid deposits in Alzheimer's disease. *Cold Spring Harb Perspect Med*. 2012;2(6):a006262. doi:10.1101/cshperspect.a006262.

36. Nuttall JR, Oteiza PI. Zinc and the aging brain. *Genes Nutr*. 2014; 9(1):379. doi:10.1007/s12263-013-0379-x.